Direct measurement of SR release flux by tracking 'Ca^{2+} spikes' in rat cardiac myocytes

Long-Sheng Song, James S. K. Sham*, Michael D. Stern, Edward G. Lakatta and Heping Cheng

*Laboratory of Cardiovascular Science, Gerontology Research Center, National Institute on Aging, National Institutes of Health, 5600 Nathan Shock Drive, Baltimore, MD 21224 and *Division of Pulmonary and Critical Care Medicine, Johns Hopkins Medical Institutions, 5501 Hopkins Bayview Circle, Baltimore, MD 21224, USA*

(Received 6 April 1998; accepted after revision 20 July 1998)

1. Ca^{2+} release flux across the sarcoplasmic reticulum (SR) during cardiac excitation–contraction coupling was investigated using a novel fluorescence method. Under whole-cell voltage-clamp conditions, rat ventricular myocytes were dialysed with a high concentration of EGTA (4·0 mM, 150 nM free Ca^{2+}), to minimize the residence time of released Ca^{2+} in the cytoplasm, and a low-affinity, fast Ca^{2+} indicator, Oregon Green 488 BAPTA-5N (OG-5N; 1·0 mM, $K_d \approx 31$ μM), to optimize the detection of localized high [Ca^{2+}] in release site microdomains. Confocal microscopy was employed to resolve intracellular [Ca^{2+}] at high spatial and temporal resolution.

2. Analytical and numerical analyses indicated that, under conditions of high EGTA concentration, the free [Ca^{2+}] change is the sum of two terms: one major term proportional to the SR release flux/Ca^{2+} influx, and the other reflecting the running integral of the released Ca^{2+}.

3. Indeed, the OG-5N transients in EGTA-containing cells consisted of a prominent spike followed by a small pedestal. The OG-5N spike closely resembled the first derivative (d[Ca^{2+}]/dt) of the conventional Ca^{2+} transient (with no EGTA), and mimicked the model-derived SR Ca^{2+} release function reported previously. In SR Ca^{2+}-depleted cells, the OG-5N transient also closely followed the waveform of L-type Ca^{2+} current (I_{Ca}). Using I_{Ca} as a known source of Ca^{2+} influx, SR flux can be calibrated *in vivo* by a linear extrapolation of the I_{Ca}-elicited OG-5N signal.

4 The OG-5N image signal was localized to discrete release sites at the Z-line level of sarcomeres, indicating that the local OG-5N spike arises from 'Ca^{2+} spikes' at transverse (T) tubule–SR junctions (due to the imbalance between calcium ions entering the cytosol and the buffer molecules).

5. Both peak SR release flux and total amount of released Ca^{2+} exhibited a bell-shaped voltage dependence. The temporal pattern of SR release also varied with membrane voltage: Ca^{2+} release was most synchronized and produced maximal peak release flux (4·2 mM s^{-1}) at 0 mV; in contrast, maximal total release occurred at −20 mV (71 *versus* 61 μM at 0 mV), but the localized release signals were partially asynchronous. Since the maximal conventional [Ca^{2+}] transient and contraction were elicited at 0 mV, it appears that not only the amount of Ca^{2+} released, but also the synchronization among release sites affects the whole-cell Ca^{2+} transient and the Ca^{2+}–myofilament interaction.

Release of Ca^{2+} from internal stores is a common pathway of intracellular signal transduction in many types of excitable and non-excitable cells, including neurons (e.g. Shmigol *et al.* 1995), oocytes (e.g. Lechleiter & Clapham, 1992), endothelial cells (Ziegelstein *et al.* 1994) and cells in plant root hairs (Ehrhardt *et al.* 1996). In mammalian ventricular myocytes, Ca^{2+} release from the sarcoplasmic reticulum (SR) constitutes a crucial step in the excitation–contraction (E–C) coupling cascade. This process is triggered by 'cross-talk' of single L-type Ca^{2+} channels to

their adjacent SR Ca^{2+} release channels or ryanodine receptors via the Ca^{2+}-induced Ca^{2+} release (CICR) mechanism (Fabiato, 1985; Stern, 1992*a*; Wier *et al.* 1994; Cannell *et al.* 1994, 1995; López-López *et al.* 1994, 1995; Sham *et al.* 1995; Adachi-Akahane *et al.* 1996), and contributes up to 90% of the cytosolic $[Ca^{2+}]$ ($[Ca^{2+}]_{cyto}$) transient (Wier *et al.* 1994; Cheng *et al.* 1994). Determination of the flux of Ca^{2+} across the SR membrane (J_{sr}) is thus essential to mechanistic studies of local and global Ca^{2+} signalling in the heart.

The conventional $[Ca^{2+}]_{cyto}$ transient is the result of several Ca^{2+} fluxes, predominantly J_{sr}, and Ca^{2+} removal processes (e.g. SR Ca^{2+}-ATPase, endogenous buffers, etc.). The J_{sr} in skeletal muscle cells has been estimated from measurements of $[Ca^{2+}]_{cyto}$ transients by explicitly accounting for Ca^{2+} removal mechanisms as well as properties of the indicator employed (Melzer *et al.* 1986; Brum *et al.* 1988; see Ríos & Pizarro, 1991, for review). Applying this generic Ca^{2+} removal model to cardiac cells, Sipido & Wier (1991) have deduced the J_{sr} of E–C coupling indirectly from the conventional $[Ca^{2+}]_{cyto}$ transient. Their studies showed that the time course of J_{sr} differs markedly from that of the $[Ca^{2+}]_{cyto}$ transient *per se*, but resembles the time derivative ($d[Ca^{2+}]_{cyto}/dt$) of the rising phase of the transient, and that the peak release flux has a bell-shaped voltage dependence with maximum of 3–5 mM s^{-1} at 0 mV. It was also emphasized that it is difficult to determine J_{sr} unequivocally by this method, due to the lack of precise information on intracellular Ca^{2+} handling (e.g. SR Ca^{2+} pump). In particular, it is dubious whether there is a steady unidirectional SR efflux during the late phase of a depolarization pulse (when the SR net flux is very small). This problem was later solved by fitting of the declining phase of the $[Ca^{2+}]_{cyto}$ transient for estimations of SR pump parameters (Balke *et al.* 1994).

The recent discovery of 'Ca^{2+} sparks' and their characterization as the elementary SR Ca^{2+} release events (Cheng *et al.* 1993; López-López *et al.* 1994, 1995; Cannell *et al.* 1994, 1995; Cheng *et al.* 1995) provides another means to quantify J_{sr}, i.e. a 'digital' SR Ca^{2+} release function can be constructed by counting discrete spark events in confocal images (Cannell *et al.* 1995; López-López *et al.* 1995; Klein *et al.* 1996). Visualization of these release events further permits study of SR Ca^{2+} release in both spatial and temporal dimensions. Unfortunately, a prerequisite of this 'digital' measurement is that these sparks should not be too frequent, to prevent overlap either spatially or temporally. To date, Ca^{2+} sparks are discernible only over a very narrow voltage range around the foot of L-type channel activation ($\leqslant -35$ mV) (Cannell *et al.* 1995; Santana *et al.* 1996); during larger depolarizations, resolution of Ca^{2+} sparks requires the application of L-type Ca^{2+} channel blockers to reduce either the single channel conductance (e.g. Cd^{2+}; Cannell *et al.* 1994) or the availability of the channel (e.g. verapmil or D600; Cheng *et al.* 1995; López-López *et al.* 1995).

In the present study, we developed a new fluorescence method to measure directly J_{sr} in confocal images without partial inhibition of L-type Ca^{2+} channels. Our approach made use of a combination of a fast, low-affinity indicator, Oregon Green 488 BAPTA-5N (OG-5N), and a high concentration of a slow, non-fluorescent Ca^{2+} chelator, EGTA. The conditions were chosen to minimize the residence time of free released Ca^{2+} in the cytoplasm and to optimize the detection of high $[Ca^{2+}]$ in the vicinity of localized release sites. Under our experimental conditions, the fluorescence transient signal consists of a prominent spike directly proportional to J_{sr} and a small component reflecting the time integral of J_{sr} (i.e. the total amount of Ca^{2+} released). This novel technique affords characterization of local and global SR Ca^{2+} release function over the entire physiological voltage range. A novel finding employing this method is that the extent of synchronization among release sites, as well as the total amount of release, is an important, heretofore unrecognized determinant of the peak $[Ca^{2+}]_{cyto}$ transient and contraction amplitude.

METHODS

Cell preparation

Ventricular cardiac myocytes were isolated from adult Sprague–Dawley rats (2–3 months old; weight, 225–300 g) using standard enzymatic techniques, as described previously (Spurgeon *et al.* 1990). Briefly, following anaesthesia (sodium pentobarbital, 100 mg kg^{-1} injected I.P.), the heart was removed from the chest and perfused retrogradely via the aorta using the Langendorff method and collagenase (Worthington Type II, 1 mg ml^{-1}). Following this perfusion procedure, single cells were shaken loose from the heart and stored in Hepes-buffered solution containing (mM): 137 NaCl, 5·4 KCl, 1·2 $MgCl_2$, 1 NaH_2PO_4, 1 $CaCl_2$, 20 glucose and 20 Hepes (pH 7·4).

Confocal microscopy

Myocytes were placed on the stage of a Zeiss LSM-410 inverted confocal microscope (Carl Zeiss, Inc., Germany) and excited by the 488 nm line of an argon laser. All image data were taken in the line-scanning mode, with the scan line usually oriented along the long axis of the myocyte, while the cell nucleus was excluded from the line. Each image consisted of 512 linescans (2·09 ms per linescan) and each line consisted of 512 pixels spaced at 0·104 μm intervals. The microscope objective was a Zeiss Plan-Neofluar ×40 oil immersion lens (NA, 1·3), and the confocal pinhole was set to render spatial resolutions of 0·4 μm in the horizontal plane and 0·9 μm in the axial direction, except in experiments shown in Fig. 5, in which the pinhole diameter was enlarged to render a 2-fold increase in focus depth. Image processing, data analysis and presentation were made using IDL software (Research Systems, Boulder, CO, USA).

Simultaneous electrophysiological recording of I_{Ca} and confocal imaging

The whole-cell patch-clamp technique was employed in conjunction with confocal imaging. Patch pipette filling solutions of designated EGTA concentrations (0, 2, 4 or 10 mM) were made by mixing, in appropriate proportions, the following two solutions: an EGTA-free solution containing (mM): 120 CsCl, 1·5 $MgCl_2$, 5 MgATP, 10 NaCl, 10 TEACl, and 20 Hepes (pH 7·2 adjusted with CsOH); and an

EGTA-containing solution containing (mM): 100 CsCl, 1·5 $MgCl_2$, 5 MgATP, 10 NaCl, 10 TEACl, 10 EGTA, 5 $CaCl_2$, and 20 Hepes (pH 7·2 adjusted with CsOH). The reduction of CsCl in the latter solution was to compensate for the osmolarity change due to EGTA and $CaCl_2$, and the additional CsOH required for pH adjustment. Assuming a K_d value of 150 nM for EGTA at pH 7·2, the free $[Ca^{2+}]$ in the EGTA-containing solutions was 150 nM. The Ca^{2+} indicator Oregon Green 488 BAPTA-5N (OG-5N) hexapotassium salt (Molecular Probes, lot 5561, 1 mM) was directly dissolved in the pipette solution and then backfilled into glass microelectrodes with resistances of 1·5–2·5 MΩ. An Axopatch 200B patch-clamp amplifier (Axon Instruments) was used for electrophysiological recordings. Following the establishment of voltage control of the cell, the local cell perfusion solution was switched to a recording solution at room temperature (22–24 °C) containing (mM): 137 NaCl, 5·4 CsCl, 1·2 $MgCl_2$, 1 NaH_2PO_4, 2 $CaCl_2$, 20 glucose, 0·01 TTX, and 20 Hepes (pH 7·4). After a period of ~5 min to allow adequate intracellular dialysis, the L-type Ca^{2+} current and SR Ca^{2+} release were activated by a series of 200 ms depolarizations from a holding potential of −60 mV to test pulses ranging from −50 to +60 mV. The magnitude of the Ca^{2+} current was indexed by the difference between the peak inward current and the current at the end of the 200 ms pulse. The voltage pulses were applied every 10 or 15 s and confocal images were acquired simultaneously; the exact timing of voltage pulse was marked on a second image channel by a 2 ms flash from a light-emitting diode.

In some experiments, Cd^{2+} (100 μM) or caffeine (10 mM) was used to block L-type channels or to empty the SR of Ca^{2+}, respectively. In our preliminary experiments, we varied the EGTA concentration while maintaining free Ca^{2+} at 150 nM and OG-5N concentrations constant in order to determine the optimal conditions for resolving the J_{sr}-related transient (see Results). Similar results were obtained at 4 and 10 mM EGTA, albeit the signal-to-noise ratio of image data was noticeably degraded at the higher EGTA concentration. In the presence of 2 mM EGTA, however, residual cell contractions were still visible following the voltage pulse in some cells, indicating that the global $[Ca^{2+}]_{cyto}$ was not sufficiently suppressed. We therefore used 4 mM EGTA mixed with 1 mM OG-5N in all experiments, except those presented in Fig. 2.

In vitro properties of the Ca^{2+} indicator OG-5N

In the present study, the low-affinity Ca^{2+} indicator OG-5N was used to measure Ca^{2+} release flux as well as conventional $[Ca^{2+}]_{cyto}$ transients. An *in vitro* calibration curve for OG-5N fluorescence intensity as a function of free $[Ca^{2+}]$ was determined on-stage using solutions containing free $[Ca^{2+}]$ of 1 μM to 1 mM (Ca^{2+} buffer kit no. 3, Molecular Probes) and 1 mM Mg^{2+}. As shown in Fig. 1, the OG-5N signal was well described by the following equation:

$$[Ca^{2+}]_{free} = K_d \frac{(F - F_{min})}{(F_{max} - F)}, \quad (1)$$

where K_d denotes the dissociation constant, and F_{max} and F_{min} the fluorescence intensity at saturating and zero $[Ca^{2+}]$, respectively. This fitting yielded a K_d of 31·4 μM and an F_{max}/F_{min} of 34, comparable with values reported by Molecular Probes ($K_d \approx 20$ μM, $F_{max}/F_{min} \approx 44$). Nearly identical results were obtained in the absence of Mg^{2+} (data not shown). Utilizing the pseudo-ratio method described previously (Cheng *et al.* 1993), the absolute $[Ca^{2+}]$ in cell experiments can be estimated from the fold increase in OG-5N fluorescence intensity ($R = F/F_0$, where F_0 is the prestimulus value of F), the *in vitro* measured K_d and R_{max} ($R_{max} = F_{max}/F_{min}$), and an assumed resting $[Ca^{2+}]$ ($[Ca^{2+}]_0$):

$$[Ca^{2+}] = K_d \frac{K_d + [Ca^{2+}]_0 - (K_d + [Ca^{2+}]_0 R_{max})R}{(K_d + [Ca^{2+}]_0 R_{max})R - (K_d + [Ca^{2+}]_0)R_{max}}. \quad (2)$$

Conversion of J_{sr} between different units

In this report, J_{sr} is expressed in three interconvertible units. The raw data are given by the dimensionless $\Delta F/F_0$ of the OG-5N signal. The OG-5N signal was calibrated by determining the conversion factor between $\Delta F/F_0$ and I_{Ca} (in the absence of SR Ca^{2+} release; 41·7 nA per 1 unit $\Delta F/F_0$, see Results). From this, the SR release fluxes are presented as the amount of equivalent Ca^{2+} current (I_{sr}), having units of nanoamps. To compare our results with those of Sipido & Wier (1991), we further employed the same conversion procedure suggested by these authors. In brief, all cells were assumed to be of the scaled geometry of a standard cell of dimensions 150 μm long, 35 μm wide and 7·5 μm thick. The volume (V) of a given cell was estimated from the membrane capacitance (C_m) of the cell, standard cell volume (V_s) and standard membrane capacitance ($C_{m,s}$, 167 pF) according to the formula:

$$V = V_s \left(\frac{C_m}{C_{m,s}}\right)^{3/2}. \quad (3)$$

The following equation was then applied:

$$J_{sr} = \frac{I_{sr}}{0{\cdot}5ZFV}, \quad (4)$$

where the number 0·5 refers to the fraction of cell volume accessible to Ca^{2+}, Z is the valence of the calcium ion, and F is the Faraday

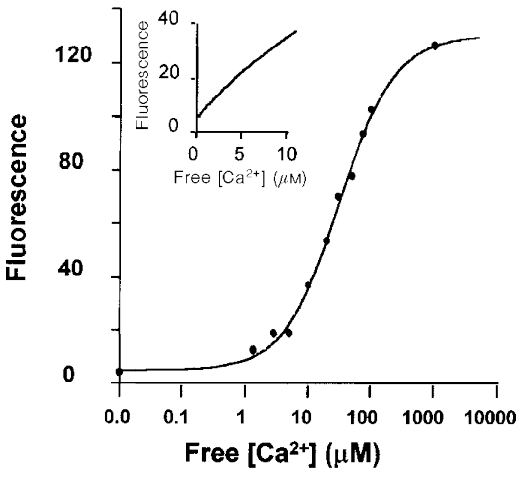

Figure 1. Semi-logarithmic plot of OG-5N fluorescence intensity as a function of free $[Ca^{2+}]$

The smooth curve is the best fit of the data using eqn (1) described in Methods, yielding a K_d of 31·4 μM and F_{max}/F_{min} of 34. Inset shows OG-5N fluorescence intensity over a range of Ca^{2+} concentrations from 0 to 10 μM on a linear scale. A calcium buffer kit for low-affinity indicators was used with the addition of 1 mM $MgCl_2$ and 20 μM OG-5N dye.

constant. The final J_{sr} would thus possess units of millimolar per second. Accordingly, the total amount of Ca^{2+} released, or the integral of J_{sr}, is reported in either $\Delta F/F_0$ or micromolar units.

Statistics

Data are reported as means ± S.E.M. Student's t test or paired t test was applied, when appropriate, to determine differences between mean values. A P value of $< 0{\cdot}05$ was taken as the statistical significance level.

RESULTS

Detection of Ca^{2+} flux associated with a 'Ca^{2+} spike': the strategy

Injection of Ca^{2+} into a buffer-containing medium, such as the cytosol, would produce a surge in free [Ca^{2+}], dubbed a 'Ca^{2+} spike', which arises from a kinetic imbalance between calcium ions and the buffer. This phenomenon has been documented experimentally in the context of rapid photorelease of Ca^{2+} from caged compounds (Escobar *et al.* 1995). We therefore proposed that tracking 'Ca^{2+} spikes' during cardiac E–C coupling may afford a novel means for direct measurement of the SR Ca^{2+} release flux. To provide the tracking mechanism, we devised a combination of a fast Ca^{2+} indicator such as OG-5N with a slow Ca^{2+} chelator such as EGTA. Intuitively, the inclusion of a slow buffer as the Ca^{2+} scavenger would reduce the residence time of released free Ca^{2+}, so that the Ca^{2+} spike would be shaped to follow closely the waveform of the injecting flux, but without being abolished altogether. In quantifying the relationship between the magnitude of Ca^{2+} flux and the amplitude of the resultant Ca^{2+} spike, our analytical results (see Appendix) revealed that in the presence of a high concentration of the slow buffer EGTA, changes in free [Ca^{2+}] (Δ[Ca^{2+}]) are composed of two terms, a major spike term proportional to the input Ca^{2+} flux, and a minor one proportional to its time integral:

$$\Delta[Ca^{2+}](t) = \frac{(K_d + [Ca^{2+}]_0)\left(\frac{(K_d + [Ca^{2+}]_0)\int_0^t J(\tau)\,d\tau}{K_d} + \frac{J(t)}{K_{off}}\right)}{[EGTA]}. \quad (5)$$

The choice of a linear, fast Ca^{2+} indicator such as OG-5N is crucial to detection of the EGTA-shaped Ca^{2+} spikes. The high K_d value of OG-5N favours the detection of high

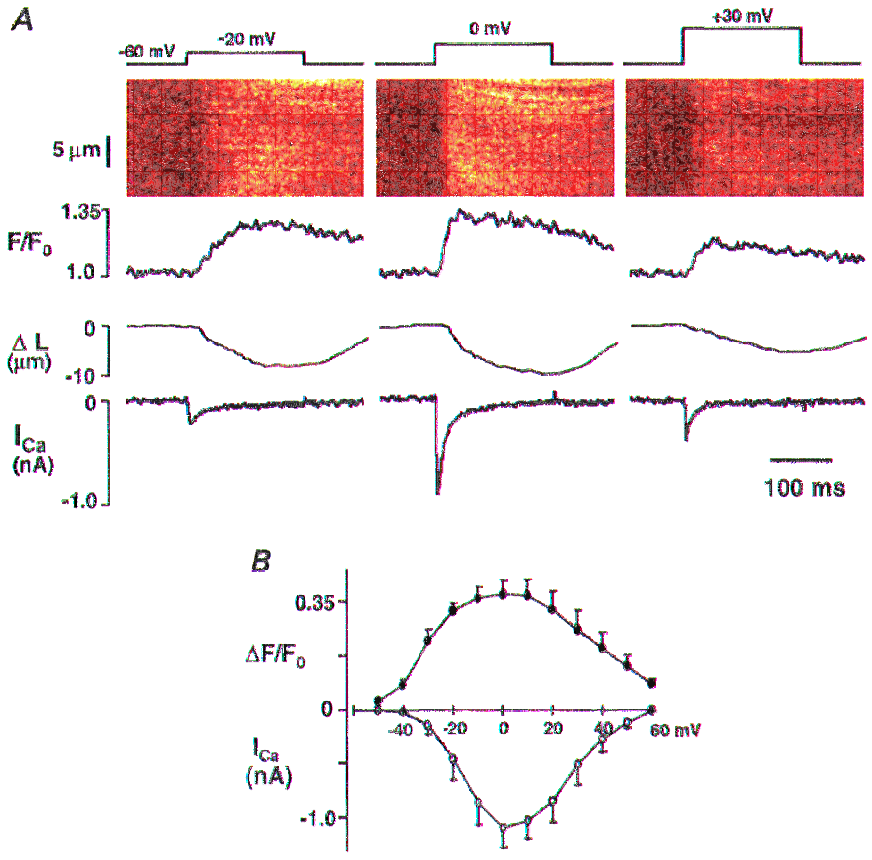

Figure 2. Conventional $[Ca^{2+}]_{cyto}$ transient measured with OG-5N (1 mM) in the absence of EGTA

A, simultaneous recording of confocal image, cell length and I_{Ca} in a representative rat ventricular myocyte. From top to bottom: voltage-clamp protocol, confocal linescan image of OG-5N fluorescence, spatially averaged OG-5N fluorescence transient normalized by its prestimulus level (F/F_0), shortening of cell length (ΔL) and I_{Ca}. Columns from left to right show results recorded on depolarization to −20, 0 and +30 mV. *B*, average peak fluorescence increases ($\Delta F/F_0$) and peak I_{Ca} from 6 cells plotted against membrane voltage.

$[Ca^{2+}]_{cyto}$ in the microdomains of release sites and yields a good linear relation between fluorescence intensity and Ca^{2+} concentration (inset of Fig. 1). The linearity not only is a convenient feature for interpretation of the experimental data but also eliminates errors in measuring non-uniform $[Ca^{2+}]_{cyto}$ (Wier *et al.* 1987; Cheng *et al.* 1993; Cannell *et al.* 1994) due to dye saturation and non-linearity (Yue & Wier, 1985). Moreover, a higher K_d usually implicates a faster Ca^{2+} dissociation rate; a fast off-rate is advantageous for tracking a rapid onset and decline of local Ca^{2+} release, so that no deconvolution is necessary to restore the true kinetics of the signal. In this respect, a closely related low-affinity dye, Calcium Orange-5N ($K_d = 53\ \mu$M), has been shown to be superior to fluo-3 ($K_d = 0{\cdot}75\ \mu$M) in tracking the rapid decline of Ca^{2+} pulses generated by photolysis of caged Ca^{2+} (fluorescence relaxation time, 143 μs *versus* 5·9 ms) (Escobar *et al.* 1995). The dye OG-5N has the extra advantage of a much higher F_{max}/F_{min} than Calcium Orange-5N (3·4), an important feature for achieving better signal contrast and signal-to-noise ratio, and thereby optimizing the spatiotemporal resolution of a weak image signal. Another similar dye, Calcium Green-5N ($K_d \approx 14\ \mu$M, $F_{max}/F_{min} \approx 38$, technical information from Molecular Probes) has been used successfully in detecting intra-sarcomeric $[Ca^{2+}]_{cyto}$ gradients in skeletal muscle cells (Escobar *et al.* 1994).

$[Ca^{2+}]_{cyto}$ transients measured with OG-5N in the absence of EGTA

Before experimentally testing the idea that OG-5N combined with EGTA can track the SR release flux, we first measured conventional $[Ca^{2+}]_{cyto}$ transients in rat ventricular myocytes using OG-5N in the absence of EGTA. Figure 2*A* shows results obtained in a representative cell with 1 mM OG-5N dialysed via the patch pipette. Each column shows, from top to bottom, membrane voltage, confocal linescan image, spatially averaged OG-5N fluorescence (F/F_0), shortening of cell length (ΔL) and simultaneously recorded I_{Ca}. Depolarization to 0 mV (middle column) elicited the maximal amplitudes of the OG-5N fluorescence transient and cell contraction. The OG-5N transient reached a peak F/F_0 value of $1{\cdot}37 \pm 0{\cdot}05$ in $46{\cdot}3 \pm 4{\cdot}8$ ms and declined with a half-decay time ($t_{½}$) of $192 \pm 5{\cdot}1$ ms ($n = 5$). Using eqn (2) and assuming $K_d = 31{\cdot}4\ \mu$M and $F_{max}/F_{min} = 34$ for OG-5N (Fig. 1), and a resting $[Ca^{2+}]_{cyto}$ of 150 nM, this 37% increase in fluorescence intensity corresponds to a peak $[Ca^{2+}]_{cyto}$ of 566 nM, which is within the range of the values reported previously in cardiac myocytes (0·4–1·5 μM; see Bers, 1991, for review). Figure 2*B* shows the bell-shaped curve for peak $\Delta F/F_0$ as a function of membrane voltage, mirrored by the current–voltage plot for I_{Ca}. These measurements using OG-5N are thus in agreement with results in the literature obtained using other indicators (Cannell *et al.* 1987; Beuckelmann & Wier, 1988; Cleemann & Morad, 1991).

OG-5N transients in the presence of EGTA

When 4 mM EGTA (2 mM total Ca^{2+} and 150 nM free Ca^{2+}) was co-dialysed with the Ca^{2+} indicator, cell contraction was completely inhibited (data not shown). The most striking observation, however, was that the configuration of the OG-5N fluorescence transient (Fig. 3, F/F_0) was distinctly different from that in the absence of EGTA. The OG-5N transient elicited by depolarization to middle-range voltages

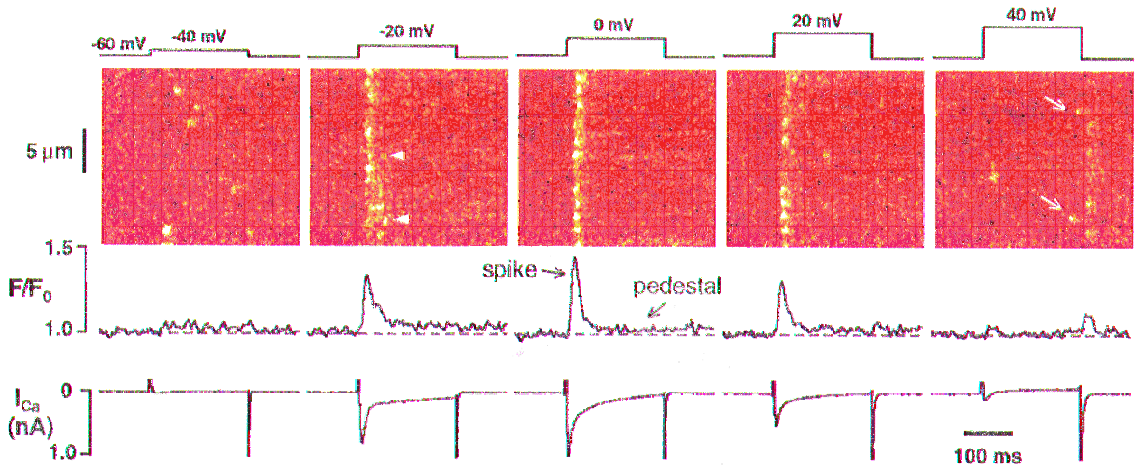

Figure 3. OG-5N fluorescence transients in the presence of EGTA

The experimental conditions were the same as in Fig. 2, except that 4 mM EGTA (with 2 mM $CaCl_2$ to retain 150 nM free Ca^{2+}) was included in the pipette filling solution and the trace for cell length change was omitted because EGTA totally suppressed cell contraction. Results from left to right were obtained at −40, −20, 0, +20 and +40 mV. Note that the OG-5N signal exhibits a brisk inital 'spike' component and a 'pedestal' component, except at extreme voltages (see Fig. 6 for further analysis). Arrowheads in the image at −20 mV mark probable events of repetitive activation at the same release sites. Arrows at +40 mV mark release events late into the depolarization pulse. Note also release events accompanying repolarization at +20 and +40 mV.

(e.g. −20, 0 and +20 mV) exhibited a prominent initial spike followed by a small, sustained pedestal that lasted beyond the depolarization pulse. At extreme voltages (e.g. −40 or +40 mV), the OG-5N transient displayed a flat waveform. The OG-5N spike at 0 mV had a time to peak (T_{peak}) of 13·1 ± 1·3 ms and a $t_{½}$ of 10·5 ± 0·46 ms ($n = 7$), which was abbreviated 18-fold compared with the $t_{½}$ of the conventional transient in the absence of EGTA. It is particularly noteworthy that this brisk OG-5N spike is reminiscent of the previously reported SR Ca^{2+} release function (Fig. 8 in Sipido & Wier, 1991). This observation supports the idea that the OG-5N spike in the presence of EGTA is related to Ca^{2+} fluxes (mainly J_{sr}) into the cytosol–OG-5N–EGTA medium, rather than to the conventional, global $[Ca^{2+}]_{cyto}$ transient.

In contrast, the pedestal component of the OG-5N transient, which reflects a quasi-steady-state increase in global $[Ca^{2+}]_{cyto}$, displayed an extremely slow relaxation, during the sustained depolarization and after repolarization (Fig. 3, see also Fig. 5). This indicates that the rate of cytosolic Ca^{2+} removal by the SR and sarcolemmal Ca^{2+} transport mechanisms was negligible under these experimental conditions, presumably because of the large quantity of Ca^{2+} buffer in the cytosol and the small elevation in $[Ca^{2+}]_{cyto}$. (As we will demonstrate later, this condition further simplifies the detection of SR unidirectional release flux during E–C coupling.) The pedestal level at 0 mV was only 0·020 ± 0·004 $\Delta F/F_0$ units or $\Delta[Ca^{2+}]_{cyto}$ of 22 nM (see eqn (2) and Fig. 5), indicating that global elevation in $[Ca^{2+}]_{cyto}$ had been damped by a factor of ~20 by EGTA.

Comparison of OG-5N spike and $d[Ca^{2+}]_{cyto}/dt$ of the conventional $[Ca^{2+}]_{cyto}$ transient

During the rising phase of a conventional $[Ca^{2+}]_{cyto}$ transient, the rate of increase in $[Ca^{2+}]_{cyto}$ or $d[Ca^{2+}]_{cyto}/dt$ provides a good predictor of J_{sr} (Sipido & Wier, 1991). To further evaluate the nature of the OG-5N spike, it is therefore instructive to compare waveforms of the OG-5N signal in the presence of EGTA and $d[Ca^{2+}]_{cyto}/dt$ of the conventional transient. Figure 4*A* shows typical OG-5N transients at 0 mV with (red) and without (black) EGTA, and the dF/dt, which approximates $d[Ca^{2+}]_{cyto}/dt$, in the EGTA-free cell (green). All traces were normalized to the same peak and baseline. It is clear that general aspects of waveform for the OG-5N spike (in EGTA-containing cells) and $d[Ca^{2+}]_{cyto}/dt$ (in EGTA-free cells) are very similar, as evidenced by similar ascending and descending rates and a nearly identical T_{peak}. Figure 4*B* shows that over a wide range of membrane potentials, T_{peak} curves for OG-5N spike and $d[Ca^{2+}]_{cyto}/dt$ overlapped each other, both exhibiting a U-shaped voltage dependence centred around 0 mV. However, T_{90} for the OG-5N spike (time from onset to 90% decay towards the pedestal level) was consistently higher

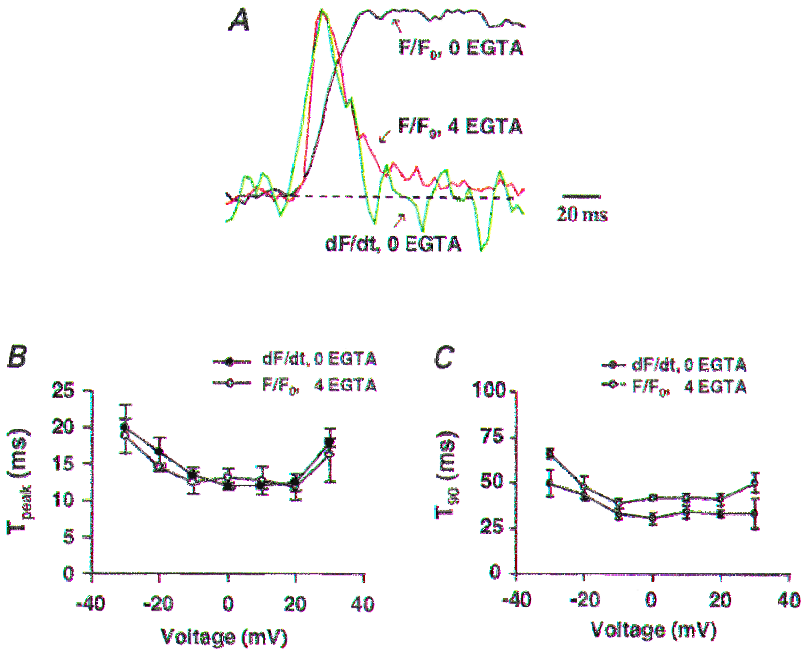

Figure 4. Waveform of the OG-5N transient in the presence of EGTA compared with the waveform of dF/dt of the OG-5N transient in an EGTA-free cell

A, typical conventional $[Ca^{2+}]_{cyto}$ transient elicited by depolarization to 0 mV and its first derivative, shown in red and green, respectively. The black trace shows the OG-5N transient in another cell in the presence of 4 mM EGTA. Dashed line indicates the baseline level. *B* and *C*, kinetic parameters of the OG-5N transient (with 4 mM EGTA) and dF/dt (with no EGTA). In *B*, T_{peak} refers to time to peak. In *C*, T_{90} refers to time from peak to 90% decay to pedestal (for OG-5N transient with EGTA) or to baseline (for dF/dt, indicated by the dashed line in *A*).

than that for $d[Ca^{2+}]_{cyto}/dt$ (time from onset to 90% decay towards the baseline level; Fig. 4*C*). The latter result is not unexpected, because when Ca^{2+} removal outweighs release, $d[Ca^{2+}]_{cyto}/dt$ eventually becomes negative during the descending phase of the $[Ca^{2+}]_{cyto}$ transient and therefore deviates from a true SR Ca^{2+} release function. The kinetic similarities between the OG-5N spike and $d[Ca^{2+}]_{cyto}/dt$ in the early phase of the $[Ca^{2+}]_{cyto}$ transient further support the notion that the spike component of the OG-5N transient reports the SR Ca^{2+} release function under these conditions.

OG-5N transient produced by Ca^{2+} influx via I_{Ca}

To test rigorously the idea that the OG-5N spike tracks J_{sr} and to quantify the relation between the magnitude of the OG-5N spike and the magnitude of J_{sr}, we examined the OG-5N response to a known source of Ca^{2+} flux, i.e. I_{Ca} injected into the cytosol. In these experiments, SR Ca^{2+} stores were depleted by 10 mM caffeine applied continuously in the perfusion solution. To maintain an adequate signal-to-noise ratio for resolving the I_{Ca}-induced OG-5N transient, the focus depth was enlarged 2-fold (to enhance photon collection efficiency) and traces obtained with the same voltage protocol were signal averaged. The I_{Ca} after SR depletion ($0{\cdot}78 \pm 0{\cdot}14$ nA, $n = 5$) was slightly, but not significantly, smaller than under control conditions ($0{\cdot}92 \pm 0{\cdot}19$ nA, $n = 5$), and elicited a tiny (< 2%) increase in OG-5N signal ($\Delta F/F_0 = 0{\cdot}017 \pm 0{\cdot}003$, $n = 5$), which was only 6% of the peak OG-5N signal prior to caffeine application ($0{\cdot}30 \pm 0{\cdot}05$, $n = 5$) (Fig. 5*A*). Concomitantly, the time constant of the fast component of L-type Ca^{2+} channel inactivation, which is sensitive to Ca^{2+} release from the SR (Sham *et al.* 1995; Adachi-Akahane *et al.* 1996; Sham, 1997), was increased by 2·4-fold, from $6{\cdot}7 \pm 0{\cdot}64$ ms under control conditions to $15{\cdot}9 \pm 2{\cdot}9$ ms ($n = 5$, $P < 0{\cdot}05$) in the presence of caffeine (Fig. 5*B*). Figure 5*C* shows representative results for the overlay of the inverted I_{Ca} (smooth trace) and the OG-5N transient (noisy trace) in the presence of caffeine. The optically recorded OG-5N transient closely tracks the waveform of the electrophysiologically recorded I_{Ca}; after subtraction of a component related to the integral of I_{Ca} (see below), the two traces almost perfectly overlap each other (Fig. 5*D*). Addition of 100 μM Cd^{2+} completely abolished both I_{Ca} and the OG-5N transients (data not shown), confirming the I_{Ca} origin of the OG-5N signal.

Several important conclusions can be drawn from these observations. (1) OG-5N combined with EGTA does indeed track Ca^{2+}fluxes into the cytosol. The OG-5N signal appears to be linearly related to the magnitude of Ca^{2+} flux. (2) Absolute calibration of the optical signal of release flux during E–C coupling can be made by a linear extrapolation of results obtained from I_{Ca} (see Discussion). The conversion factor measured in five cells was, on average, $41{\cdot}7 \pm 5{\cdot}7$ nA per unit increment of $\Delta F/F_0$. (3) I_{Ca} contributes little to the OG-5N signal when the SR is intact. This is, in part, because I_{Ca} inactivation would be hastened by SR Ca^{2+} release, contributing even smaller total flux than was observed with the SR empty.

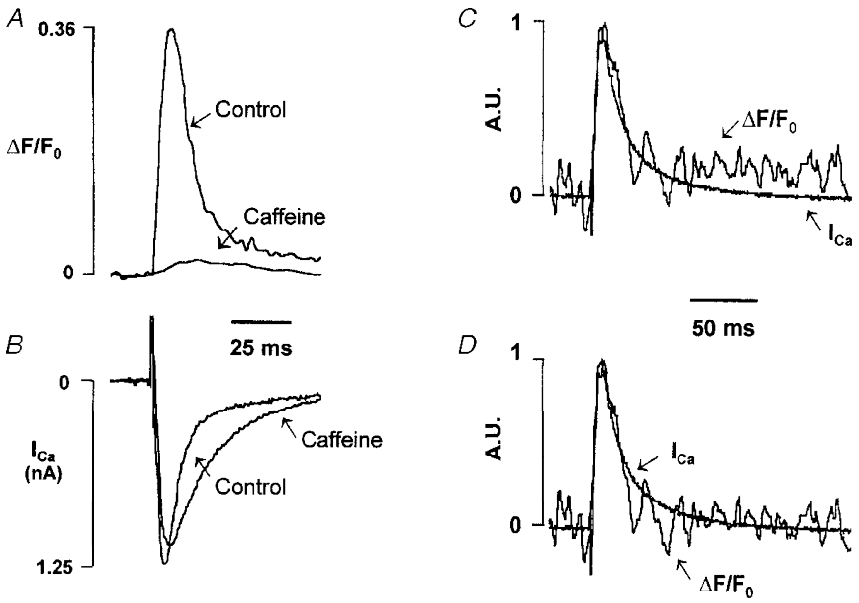

Figure 5. Typical OG-5N transient evoked by Ca^{2+} influx through L-type channels

A and *B*, OG-5N transients (*A*) and I_{Ca} (*B*) at 0 mV before (Control) and after 10 mM caffeine. The OG-5N signal in the presence of caffeine was averaged from 5 consecutive recordings. *C*, OG-5N transient (noisy trace) obtained in the presence of caffeine was scaled and superimposed on the inverted I_{Ca} (A.U., arbitrary units). *D*, same as in *C* except that the integral component of the OG-5N transient was subtracted ($\alpha = 6{\cdot}0\ s^{-1}$). See the text for the algorithm.

Separation of the OG-5N signal into the flux- and integral-related components

The above theoretical and experimental results indicate that the OG-5N transient in the presence of EGTA can be subdivided into two components: a prominent spike directly related to Ca^{2+} flux (f_r) and a small component representing the running integral of the flux (f_s). That is,

$$\Delta F/F_0 = f_r + f_s. \quad (6)$$

Considering eqn (5) and taking the OG-5N signal as a linear measurement of instantaneous $[Ca^{2+}]_{cyto}$, we have:

$$f_s = \alpha \int_0^t f_r \mathrm{d}t, \quad (7)$$

where:

$$\alpha = K_{off}\left(1 + \frac{[Ca^{2+}]_0}{K_d}\right). \quad (8)$$

Thus, α is a constant determined mainly by the dissociation constant, K_d, and off-rate, K_{off}, of EGTA, but appears to be independent of EGTA concentration in the high EGTA limit. Experimentally, the single parameter α was determined by fitting f_s to the pedestal level after repolarization from 0 mV, when J_{sr}, I_{Ca} and thereby f_r are expected to be zero. The same α value was subsequently applied to all traces obtained in the same cell, including the repolarization-elicited releases following strong depolarization (see below). Strictly speaking, sources of Ca^{2+} fluxes for f_r should include input fluxes from sources other than J_{sr}, such as I_{Ca} (Fig. 5) and, at strong depolarizations, possibly the reverse mode Na^+–Ca^{2+} exchange (Beuckelmann & Wier, 1989; Crespo *et al.* 1990). However, in most situations, these sarcolemmal influxes are small relative to J_{sr} (Fig. 5; Wier, 1990; Sipido & Wier, 1991; Cleemann & Morad, 1991), so we will use f_r and J_{sr} interchangeably unless otherwise indicated. Similarly, Ca^{2+} clearance during the pulse by transporting mechanisms, which represents a negative unidirectional Ca^{2+} flux, is neglected because it is extremely slow (Fig. 3).

Voltage dependence of SR release: peak flux, total release and temporal pattern

Figure 6*A* shows traces of OG-5N transients obtained in the same cell at −40, −20, 0, +20, +40 and +60 mV. Applying

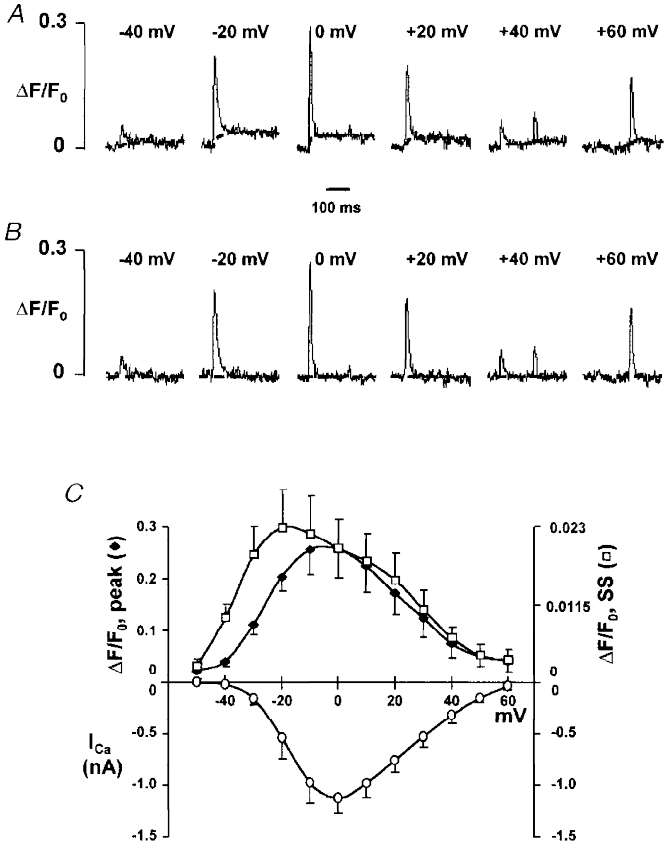

Figure 6. Time course and voltage dependence of SR Ca^{2+} release

A, OG-5N transients measured at −40, −20, 0, 20, 40 and 60 mV (from left to right) in a different cell from that in Fig. 3. The dashed lines represent the integral component f_s. *B*, release functions f_r or J_{sr} were obtained by subtracting f_s from the original records using the algorithm described in the text ($\alpha = 5{\cdot}5\ s^{-1}$) (horizontal dashed lines indicate the zero level). *C*, average voltage dependence of peak release, integral of release (SS) and peak I_{Ca} from the same cells. The total release and the peak J_{sr} curves were scaled so that they matched at 0 mV.

the algorithm described above, the value of α was determined to be 5·5 s^{-1} in this cell (varying from 4·8 to 6·7 s^{-1} in 5 other cells). The dissected running integral component, f_s, is shown as the dashed lines in Fig. 6*A*, and the concurrent SR release component, f_r, is shown in Fig. 6*B*. The SR release was detectable at −40 mV, reached a maximum at 0 mV, and then decreased with further depolarization until virtually vanishing at +60 mV. For test potentials beyond +20 mV, repolarization also activated SR Ca^{2+} release, in agreement with previous observations that the tail I_{Ca} of repolarization triggers a tail $[Ca^{2+}]_{cyto}$ transient (Cannell *et al.* 1987; Beuckelmann & Wier, 1988; Cleemann & Morad, 1991). The maximal $\Delta F/F_0$ of the OG-5N spike was 0·25 ± 0·04 ($n = 7$), which represents a Ca^{2+} flux equivalent to a Ca^{2+} current of 10·5 nA. Given the measured cell membrane capacitance ($C_m = 111 \pm 16{\cdot}9$ pF, $n = 7$), and using the conversion procedure described in Methods, this translated into a peak J_{sr} of 4·6 mM s^{-1} or 4·2 mM s^{-1} after subtracting I_{Ca} flux. This value of peak J_{sr} is thus highly comparable to that inferred from the $[Ca^{2+}]_{cyto}$ transient (3–5 mM s^{-1} in guinea-pig heart cells at 0 mV; Sipido & Wier, 1991; Balke *et al.* 1994). It is important to note that the time integral of the release (f_s at pedestal) reached its maximum of 0·023 $\Delta F/F_0$ units or 70·5 μM at −20 mV rather than at 0 mV (0·020 $\Delta F/F_0$ units or 61·3 μM). The values for maximal cumulative SR Ca^{2+} release at 0 mV are also similar to those reported previously (Sipido & Wier, 1991; Balke *et al.* 1994).

We next compared the voltage dependence of peak J_{sr}, of the total SR release, and of the peak I_{Ca} (Fig. 6*C*). Curves for peak J_{sr} and total release were scaled and aligned vertically at 0 mV. Although both peak and total SR release were bell shaped, they were notably different, with the largest discrepancies occurring at negative potentials. For

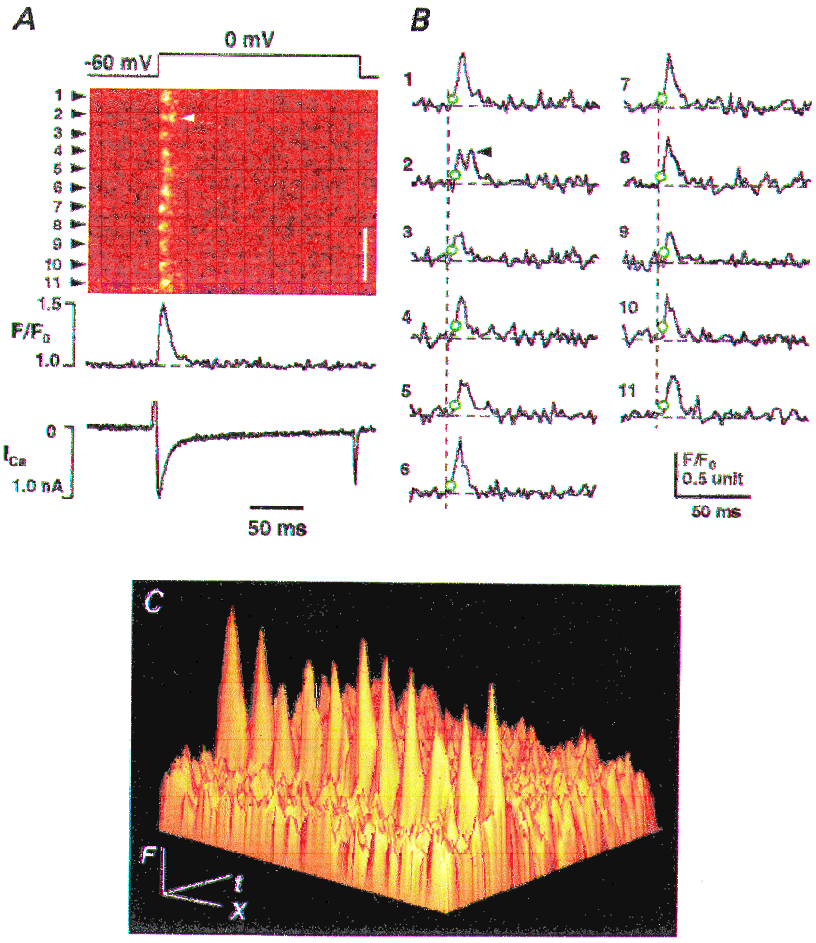

Figure 7. Visualization of TT–SR diadic release events during a large J_{sr}

A, confocal images showing discrete TT–SR release events at 11 sarcomeres (arrowheads), release function (with the integral component subtracted) and I_{Ca}. Depolarization voltage was 0 mV (top). Arrowhead in the image shows what probably represents a reopening subsequent the first opening. Scale bar: 5 μm. *B*, release function at individual TT–SR sites. The dashed lines show the onset of depolarization and the open circles indicate the activation of individual TT–SR sites. *C*, data in *A* are shown as a 3-D plot of fluorescence (F), time (t) and space (X). Upon depolarization, the OG-5N fluorescence peaks sharply at the level of the Z-lines, but no detectable increase is observed at centre regions between Z-lines, locations from which the SR Ca^{2+} release apparatus is probably excluded.

example, the maximum for total release was observed at −20 mV rather than at 0 mV at which J_{sr} peaked; the total releases at −30 mV and at 0 mV were about the same but the peak J_{sr} at −30 mV was 45% less than that at 0 mV. These results indicate that the peak release does not always reflect the total release. Moreover, it is noteworthy that the curves for both peak and total release were shifted leftwards in relation to the peak I_{Ca}–V curve, in agreement with previous results (Cannell *et al.* 1987; Cleemann & Morad, 1991; Wier *et al.* 1994).

We also examined the temporal spreading of the SR activation at different voltages. At −40 mV, discrete release events were sporadic and occurred at any time during the pulse. Spatial averaging resulted in a small, flat OG-5N transient (Fig. 3). However, release events at middle-range voltages (−20 to +20 mV) were clustered to the early part of the pulse, and were mostly synchronized at around 0 mV (Figs 3 and 7), conferring upon the OG-5N transient the distinctive spike-like appearance. Sporadic, late release events were also seen during depolarization to very positive potentials (arrowheads in Fig. 3). Tail releases, whether large or small, were all highly synchronized and, in the accompanying line plots, had rather narrow durations. This temporal pattern of SR release provides a good explanation for the aforementioned discrepancy in the voltage dependence of total SR Ca^{2+} release and peak SR release flux. Evidently, the more scattered the release (e.g. at negative potentials), the smaller the peak flux, and after integration, the larger the total amount of released Ca^{2+} relative to the peak flux.

Measuring 'Ca^{2+} spikes' at T tubule–SR diadic junctions

In addition to providing direct measurements of whole-cell J_{sr} and its integral, the present method provides detailed information on spatial and local characteristics of the SR release function. With EGTA limiting the spatial diffusion of the released Ca^{2+}, the OG-5N signal was highly localized to regular, discrete sites, which were clearly discernible, even at the largest SR release (e.g. at 0 mV; Figs 3 and 7). When the scanline was placed along the longitudinal axis of the cell, the interval between neighbouring sites was about 1·8 μm (Figs 3 and 7), roughly the slack sarcomere length, indicating that these sites probably correspond to T tubule (TT)–SR diadic junctions at the Z-lines of the sarcomeres. The intrasarcomeric gradients are more clearly illustrated in Fig. 7*C* where fluorescence intensity (F) is portrayed as a 3-dimensional plot of time (t) and space (X). This observation substantiates our conclusion that in the presence of EGTA, the OG-5N spike directly reflects the TT–SR junctional 'Ca^{2+} spikes' associated with local release, and is consistent with the fact that the elementary SR Ca^{2+} release events, Ca^{2+} sparks, occur at the TT–SR junctional regions only (Shacklock *et al.* 1995; Cheng *et al.* 1996). Hence, it is natural for the OG-5N spike to be linearly related to the J_{sr}. (Note that putative discrete OG-5N spikes due to single L-type Ca^{2+} channel currents in SR Ca^{2+}-depleted cells were too faint to be discerned by imaging (data not shown).) With the improved spatial resolution of release sites afforded by the present method, the timing and the time course of individual TT–SR diadic release (J_{sr}) can be readily resolved. Figure 7*B* shows an example of TT–SR response to depolarization to 0 mV. The onset of local releases (marked by open circles) was as fast as the time resolution of the scanning (2·1 ms or 1 linescan for labels 7 and 8). On average, the TT–SR release had a T_{peak} of 8·78 ± 0·78 ms and a T_{90} of 27·6 ± 1·33 ms ($n = 11$ sarcomeres). Usually, a given TT–SR junction could be activated only once (within the space–time resolution limit of the present method) during a test pulse. Doublet activation events at a single TT–SR junction were only occasionally observed (arrowheads in Figs 3 and 7), suggesting that individual release sites become refractory after local release. The localized refraction could be explained by inactivation (Fabiato, 1985) or 'adaptation' (Györke & Fill, 1993) of the release channels (see also Sham *et al.* 1998), but is unlikely to be due to local depletion of SR Ca^{2+} stores (because pharmacologically modified 'Ca^{2+} sparks' can last several seconds) (Cheng *et al.* 1993; Xiao *et al.* 1997).

DISCUSSION

Tracking 'Ca^{2+} spikes' by OG-5N in combination with EGTA

Utilizing a combination of OG-5N and EGTA, we have, for the first time, directly measured the SR Ca^{2+} release function underlying cardiac E–C coupling. Specifically, the OG-5N transients in the presence of EGTA were composed of two inter-related yet separable components: a major spike component directly related to Ca^{2+} fluxes into the cytosol, predominantly J_{sr}, and a minor component (< 10% of peak) related to the running integral of the fluxes. Dissection of these components required the fitting of OG-5N transients to eqns (6) and (7) (to determine the constant α), but no specific knowledge of intracellular Ca^{2+} handling was necessary. Absolute calibration of J_{sr} made use of linear extrapolation of the response of the OG-5N–EGTA–endogenous buffer system to a known Ca^{2+} source, the I_{Ca}.

The experimental evidence that the OG-5N spike (with intact SR) reflects SR Ca^{2+} release flux is compelling. Firstly, the OG-5N spike has a unique time course that resembles $d[Ca^{2+}]_{cyto}/dt$ of the conventional transient in the rising phase (Fig. 4), a rough estimator of J_{sr}, and mimicks the reported SR Ca^{2+} release function (Sipido & Wier, 1991; Balke *et al.* 1994). Other salient features of the directly resolved J_{sr}, including its magnitude and voltage dependence, are also in close agreement with those inferred from deconvolution of the $[Ca^{2+}]_{cyto}$ transient (Sipido & Wier, 1991; Balke *et al.* 1994). Secondly, in SR Ca^{2+}-depleted cells, the residual OG-5N transient (< 2% increase in OG-5N signal) due to I_{Ca} alone tracked the time course of the electrophysiologically recorded I_{Ca} (Fig. 5). The most direct evidence to support our conclusion, however, comes from confocal imaging. Regardless of the magnitude of SR

release, the OG-5N transients consisted of discrete, localized OG-5N spikes reflecting TT–SR diadic 'Ca^{2+} spikes'. As a result, the OG-5N–EGTA transient reflects the spatial and temporal summation of Ca^{2+} spikes at individual release sites, as well as the minute change in background $[Ca^{2+}]_{cyto}$ due to the continuous Ca^{2+} flux.

Although TT–SR Ca^{2+} spikes are closely related to Ca^{2+} sparks (measured with fluo-3), they are conceptually different. According to model simulation, the amplitude of Ca^{2+} sparks in the absence of EGTA depends on not only the Ca^{2+} source strength, but also the duration of release; its rate of decay after termination of release is determined by diffusion of Ca^{2+}, the mobility and kinetics of the indicator, and the exchange of Ca^{2+} between the indicator and endogenous buffers (Smith *et al.* 1998). The spikes in this study, however, are related to the *local release flux* underlying these Ca^{2+} sparks; collectively, they provide a measurement of the release function underlying the conventional $[Ca^{2+}]_{cyto}$ transients (arising from the summation of the elemental Ca^{2+} sparks). For example, the whole-cell Ca^{2+} spike at 0 mV lasts about 20 ms (at 50% peak level), whereas solitary sparks have an even longer duration (typical $T_{peak} \approx 15$ ms and $t_{½} \approx 20$ ms in ventricular myocytes) (Cheng *et al.* 1993; López-López *et al.* 1995; Xiao *et al.* 1997). Depending on the degree of TT–SR activation, a TT–SR junctional Ca^{2+} spike may or may not represent a single Ca^{2+} spark event. Future experimental studies are required to define the number of Ca^{2+} sparks involved during a junctional spike under various circumstances.

Numerical simulation of the OG-5N–EGTA–endogenous buffer system

An analytical approach detailed in the Appendix provides a theoretical basis for our utilization of OG-5N–EGTA to track Ca^{2+} fluxes into the cytosol. To further elucidate how OG-5N–EGTA works, we resorted to numerical simulation using realistic buffer kinetics and concentrations. In the simplest case, we assumed that Ca^{2+} flux of square waveform was uniformly injected into a homogeneous medium containing OG-5N, EGTA and various buffers of the characteristics of endogenous Ca^{2+}-binding sites (Fig. 8). After subtracting the running integral component

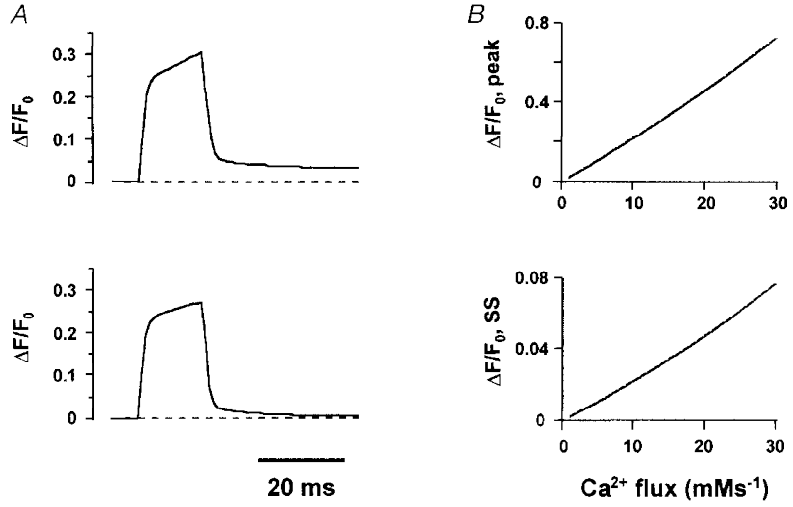

Figure 8. The OG-5N Ca^{2+} spike in the presence of a high concentration of a slow Ca^{2+} buffer: numerical simulation

The following buffer species were included in our simulation: EGTA, 4000 μM, $K_{on} = 20\ \mu M^{-1}\ s^{-1}$, $K_{off} = 3\ s^{-1}$; OG-5N, 1000 μM, $K_{on} = 323\ \mu M^{-1}\ s^{-1}$, $K_{off} = 10\,000\ s^{-1}$; calmodulin, 24 μM, $K_{on} = 100\ \mu M^{-1}\ s^{-1}$, $K_{off} = 38\ s^{-1}$; troponin C, 70 μM, $K_{on} = 39\ \mu M^{-1}\ s^{-1}$, $K_{off} = 20\ s^{-1}$; SR membrane binding sites, 47 μM, $K_{on} = 115\ \mu M^{-1}\ s^{-1}$, $K_{off} = 100\ s^{-1}$; sarcolemmal membrane binding sites, 1124 μM, $K_{on} = 115\ \mu M^{-1}\ s^{-1}$, $K_{off} = 115\,000\ s^{-1}$. The initial resting $[Ca^{2+}]$ was 150 nM. The dissociation constants for EGTA are based on its K_d (150 nM at pH7·2), the measured value of α in cells ($\sim 6\ s^{-1}$) and eqn (8). The dissociation rate for OG-5N was chosen in reflection of its K_d value (31 μM) and the result of Escobar *et al.* (1995) on a similar dye. The protein and membrane Ca^{2+}-binding parameters are integrated from data in the literature (Sipido & Wier, 1991; Weir *et al.* 1994; Langer & Peskoff, 1996). *A*, waveforms of Ca^{2+} flux (15 ms square wave, 12·5 mM s^{-1}) for the raw OG-5N transient (top), and the OG-5N transient after removal of the running integral ($\alpha = 6{\cdot}2\ s^{-1}$; bottom). The on- and off-response time is 0·8 ms measured at 50% peak level. The small creeping component seen after subtraction of the integral component reflects non-equilibrium attribution of injected Ca^{2+} among various buffers (during injection) or interchange of Ca^{2+} between EGTA and OG-5N (after termination of injection). Increasing EGTA concentration further suppressed the creeping component, and reduced the spike amplitude, but only slightly affected the value of α (data not shown). *B*, peak OG-5N spike (top) and steady-state pedestal OG-5N fluorescence (bottom) as a function of the magnitude of Ca^{2+} flux.

($\alpha = 6{\cdot}2\ s^{-1}$), the initial overshoot in OG-5N signal or OG-5N spike reproduces well the waveform of Ca^{2+} flux, with an 'on' and 'off' response time of less than 1 ms (measured at 50% peak level). More importantly, the relationships between the amplitude of the OG-5N spike, the steady-state OG-5N signal and the strength of Ca^{2+} injection are almost linear over a wide range of Ca^{2+} flux (0–30 mM s^{-1}, corresponding to peak $\Delta F/F_0$ values up to 0·8; Fig. 8*B*). These numerical results suggest that the 'high, slow buffer concentration limit' used for derivation of eqn (8) is valid under our experimental conditions. In addition, it is justifiable to use linear extrapolation of results obtained with small flux to calibrate larger flux, as we did in this study (see Results). Owing to these linear relationships, qualitatively similar results would be expected even if the source Ca^{2+} is spatially non-uniform, as occurs within cells, provided that the local release flux is below that required to produce local saturation of buffers.

Does EGTA alter J_{sr} under physiological conditions?

Within a TT–SR diadic junction, main Ca^{2+} signalling routes are thought to proceed from L-type Ca^{2+} influx to activation of the release channels; released Ca^{2+} reciprocally inactivates the L-type channels, and release channels interact with each other, all occurring at nanoscopic and microscopic scales. The inclusion of EGTA at concentrations used in the present study is, however, not expected to disturb, to a significant extent, any of these intermolecular Ca^{2+} signalling processes. In studies using millimolar concentrations of fura-2, it has been found that the SR release remains intact despite the fact that the global $[Ca^{2+}]_{cyto}$ transient is markedly reduced and cell contraction is totally abolished (Adachi-Akahane *et al.* 1996). Recently, Sham (1997) provided more direct evidence that intracellular dialysis of up to 10 mM EGTA has little effect on the release flux, as manifested by little change in the release-dependent L-type Ca^{2+} channel inactivation (Sham, 1997). A similar result was observed in the present study (data not shown). Consistent with these observations, it has been illustrated theoretically that millimolar EGTA is impotent with respect to chelation of Ca^{2+} in the vicinity of permeation pores of Ca^{2+} channels (Stern, 1992*a*,*b*). We therefore may conclude that in the present study EGTA does not alter the J_{sr}. Indeed, the absolute SR flux determined here is not different from the value obtained in the absence of excessive exogenous buffers (Sipido & Wier, 1991; Balke *et al.* 1994; Wier *et al.* 1994). Nevertheless, it should be cautioned that supramicrometre Ca^{2+} communications (e.g. possible interaction between adjacent TT–SR diads, Ca^{2+} waves) or global Ca^{2+}-mediated effects (e.g. cell contraction) could be retarded or abolished by millimolar EGTA. Another limitation imposed by EGTA is that a long interpulse interval ($\geqslant 10$ s) is necessary to ensure repletion of the SR store (as judged by a large, stable SR release in response to repetitive depolarizations to 0 mV; data not shown).

Temporal synchronization of SR release and its physiological significance

Both confocal images and line plots of J_{sr} revealed that the degree of synchronization of SR Ca^{2+} release is distinctly voltage dependent. The most synchronized release occurs at around 0 mV, as reflected by the fastest T_{peak} and the narrowest T_{90} of J_{sr}, as well as the fact that discrete TT–SR spikes clustered to the beginning of the pulse. At the negative voltage end, however, release events were activated more asynchronously, resulting in a scattered TT–SR activation and a flat J_{sr}. Interestingly, the inactivation time constants of I_{Ca} exhibit similar U-shaped voltage dependencies, with the fastest I_{Ca} observed at around 0 mV (Sham, 1997). This suggests that the SR Ca^{2+} release kinetics are tightly controlled by the activation and inactivation kinetics of L-type channels. This interpretation is in agreement with the observation that, in the presence of L-type channel blockers, activation of Ca^{2+} sparks at all voltages follows the waveform of L-type current in the presence of verapmil (López-López *et al.* 1995). However, local refractoriness after release, as shown in Fig. 7, and possibly SR Ca^{2+} depletion may provide additional mechanisms to accentuate the temporal localization of large J_{sr}.

A novel concept arising from the present results is that the synchronization among SR Ca^{2+} release sites may be of vital physiological significance in determining the effectiveness of released Ca^{2+} to activate the contractile machinery. For example, the maximal cell contraction, J_{sr} and $[Ca^{2+}]_{cyto}$ transient occur at 0 mV, at which the releases occur synchronously (Sipido & Wier, 1991; Balke *et al.* 1994; this study); in contrast, total SR Ca^{2+} release peaks around −20 mV (Fig. 6*C*), but the release is relatively unsynchronized. In addition, cells contract twice as vigorously at 0 mV as at −30 mV (data not shown), with about the same amount of released Ca^{2+} (Fig. 6). We speculate that substantial modulation of cardiac contractility can occur simply by varying the degree of synchronization of SR Ca^{2+} release.

Comparison with previous work

In general, the direct measurement of J_{sr} using the OG-5N–EGTA fluorescence method is an improvement upon the Ca^{2+} removal modelling method to estimate J_{sr} (Melzer *et al.* 1986; Brum *et al.* 1988; Sipido & Wier, 1991). As long as the high, slow buffer concentration condition is valid, it does not require cell-type specific knowledge of intrinsic Ca^{2+} transporting and buffering mechanisms. In addition, because the 'differentiation' implicit in the calculation of release flux is done by the buffer system, before the addition of photon shot noise, the signal-to-noise ratio is more favourable than in methods that determine release flux numerically from fluorescence signals that reflect $[Ca^{2+}]_{cyto}$. Possible errors due to saturation and non-linearity of the Ca^{2+} indicator (Yue & Wier, 1985) have

essentially been circumvented, and the interpretation of the experimental data is rather straightforward. The present method also extends the 'digital' Ca^{2+} spark-counting method (Cheng *et al.* 1993; Cannell *et al.* 1995; López-López *et al.* 1995; Klein *et al.* 1996) by providing continuous, absolute measurement of J_{sr} while maintaining a submicrometre spatial resolution of release origin, even at large values of J_{sr}. In contrast to the spark-counting method, this approach is also applicable when unitary properties of Ca^{2+} sparks are subjected to modulation by physiological and pharmacological mechanisms (e.g. Cheng *et al.* 1993; Xiao *et al.* 1997; Song *et al.* 1997). In skeletal muscle, the $[Ca^{2+}]_{cyto}$ transient in the presence of EGTA (15 mM) has the same general shape as the Ca^{2+} release waveform but without an apparent integral component (Ríos & Pizarro, 1991). The present results clearly show both release- and integral-related components. Our theoretical reasoning further suggests that the relative magnitude of these components (the value α) would be insensitive to EGTA concentration, provided it is sufficiently large. The reason for the absence of an integral component under the experimental conditions of Ríos & Pizarro (1991) is unclear. Transient, large intra-sarcomere $[Ca^{2+}]_{cyto}$ gradients have been observed previously in both skeletal (Escobar *et al.* 1994) and cardiac muscle cells (Isenberg *et al.* 1996). In the presence of EGTA, which serves mainly as a free-Ca^{2+} scavenger rather than as a Ca^{2+} diffusion facilitator, these gradients appeared to be further steepened under our experimental conditions (Figs 3 and 7), as evidenced by the lack of cellular contraction despite large TT–SR junctional Ca^{2+} spikes.

Similar to the previous studies (Cleemann & Morad, 1991; Wier *et al.* 1994), a leftwards shift of the SR Ca^{2+} release as a function of voltage in relation to the I_{Ca}–V curve was observed in the present study (Fig. 6*C*). This indicates that the efficacy of L-type Ca^{2+} influxes as the trigger of release decreases as membrane potential is increasingly positive. This phenomenon can now be explained on the basis that: (1) SR release is controlled locally by single L-type channel current (i_{Ca}) (Niggli & Lederer, 1990; Stern 1992*a*; Wier *et al.* 1994; Cannel *et al.* 1995; López-López *et al.* 1995; Sham *et al.* 1995; Sham, 1997); (2) the electrochemical driving force and therefore the amplitude of i_{Ca} decrease monotonically with depolarization towards the reversal potential; and importantly, (3) SR activation is a non-linear (square) function of i_{Ca} (Santana *et al.* 1996).

The intermolecular Ca^{2+} signalling at TT–SR diadic junctions has been the main focus of several recent theoretical studies (Langer & Peskoff, 1996; Soeller & Cannell, 1997). It seems that a thorough understanding of cardiac E–C coupling would ultimately rely on resolution of local Ca^{2+} signalling on submicrometre and submillisecond scales. In this regard, the present method of visualization of Ca^{2+} spikes associated with TT–SR release may provide a stepping stone towards achieving this challenging goal. Moreover, since mobilization of internal Ca^{2+} through ryanodine receptors or inositol trisphosphate receptors is a ubiquitous signalling process, this method may have general applications for studies in many other types of cell.

APPENDIX

An analytical derivation of the behaviour of Ca^{2+} under the high EGTA conditions was carried out with the assistance of the symbolic computer mathematics package Macsyma (Macsyma Corp., Arlington, MA, USA). We began with the basic equation of Ca^{2+} balance in the presence of EGTA, including a factor $b + 1$ for effective volume due to other buffers treated in the rapid buffering approximation, which is the worst case for the error due to flux on and off the fast buffers (see Discussion for a more realistic numerical simulation of fast buffer effects). The free Ca^{2+} concentration is $ca(t)$, the source flux into the cell is $J(t)$, total EGTA is egt, and $[Ca^{2+}]:[EGTA]$ is $egca(t)$:

$$\frac{\mathrm{d}ca(t)}{\mathrm{d}t} = \frac{J(t) + K_{off}\,egca(t) - K_{on}\,ca(t)(egt - egca(t))}{b+1}. \quad \text{(A1)}$$

Net Ca^{2+} balance is expressed by the following, where $bb(t)$ is Ca^{2+} bound to fast buffers (including Oregon Green), and $ig(t)$ is the running integral of $J(t)$:

$$egca(t) + ca(t) + bb(t) = ig(t) + egca_0 + ca_0 + bb_0, \quad \text{(A2)}$$

where the starting equilibrium values are given by:

$$egca_0 = \frac{ca_0\,egt\,K_{on}}{ca_0 K_{on} + K_{off}} \quad \text{(A3)}$$

and

$$bb_0 = \frac{bt\,ca_0 K_{b,on}}{ca_0\,K_{b,on} + K_{b,off}}, \quad \text{(A4)}$$

where $K_{b,on}$ and $K_{b,off}$ are association and dissociation rate constants for the fast buffers. Using eqn (A2) to replace $egca(t)$ in eqn (A1), and defining δ as the deviation of $[Ca^{2+}]$ from resting:

$$\frac{\mathrm{d}\delta}{\mathrm{d}t} = \frac{J(t) + K_{off}\left(ig(t) + \dfrac{ca_0\,egt\,K_{on}}{ca_0 K_{on} + K_{off}} - b\delta - \delta\right)}{b+1} - \frac{(\delta + ca_0)K_{on}\left(-ig(t) - \dfrac{ca_0\,egt\,K_{on}}{ca_0 K_{on} + K_{off}} + egt + b\delta + \delta\right)}{b+1}. \quad \text{(A5)}$$

Equation (A5) cannot be solved analytically because of the quadratic appearance of δ together with the unknown functions $J(t)$ and $ig(t)$. However, it is intuitively obvious (and can be proven mathematically) that the excursion of $[Ca^{2+}]$ from equilibrium, δ, can be made as small as desired by using a sufficiently large concentration of EGTA, which will also permit the total amount of Ca^{2+} entering, $ig(t)$, to

be treated as a (relatively) small quantity. Therefore, in the high EGTA conditions, we can linearize the equation in δ, J and ig, obtaining, after dropping constants which are relatively small in the high EGTA conditions, a linear differential equation with constant coefficients:

$$\frac{\mathrm{d}\delta}{\mathrm{d}t} = \frac{\left\{\dfrac{J\tau}{b+1} + \dfrac{(K_\mathrm{d} + ca_0)^2\, ig}{K_\mathrm{d}\, egt}\right\} - \delta}{\tau}, \tag{A6}$$

where:

$$\tau = \frac{(b+1)(K_\mathrm{d} + ca_0)}{egtK_\mathrm{off}}. \tag{A7}$$

This can be recognized as the equation of a single-compartment system with a source given by the quantity in curly brackets, and transient (mono-exponential) response time τ. For times and rates of change of $J(t)$ long compared with this transient response time (which itself becomes arbitrarily short in the high EGTA conditions), δ will be given by the steady-state response, which is found by setting the right-hand side of eqn (A6) to zero. After replacing δ and ig by their definitions, we find that the deviation of $[Ca^{2+}]$ from equilibrium is given by eqn (A8), identical to eqn (5) in the Results, confirming that it is the sum of two terms, one proportional to the Ca^{2+} flux/release function $J(t)$) and the other to its time integral:

$$ca(t) - ca_0 = \frac{(K_\mathrm{d} + ca_0)\left(\dfrac{(K_\mathrm{d} + ca_0)\int_0^t J(\tau)\mathrm{d}\tau}{K_\mathrm{d}} + \dfrac{J(t)}{K_\mathrm{off}}\right)}{egt}. \tag{A8}$$

Adachi-Akahane, S., Cleemann, L. & Morad, M. (1996). Cross-signaling between L-type Ca^{2+} channels and ryanodine receptors in rat ventricular myocytes. *Journal of General Physiology* **108**, 435–454.

Balke, C. W., Egan, T. M. & Wier, W. G. (1994). Processes that remove calcium from the cytoplasm during excitation–contraction coupling in intact rat heart cells. *Journal of Physiology* **474**, 447–462.

Bers, D. M. (1991). *Excitation-Contraction Coupling and Cardiac Contractile Force.* Kluwer Academic Publishers, Boston, USA.

Beuckelmann, D. J. & Wier, W. G. (1988). Mechanism of release of calcium from sarcoplasmic reticulum of guinea-pig cardiac cells. *Journal of Physiology* **405**, 233–255.

Beuckelmann, D. J. & Wier, W. G. (1989). Sodium–calcium exchange in guinea-pig cardiac cells: exchange current and changes in intracellular Ca^{2+}. *Journal of Physiology* **414**, 499–520.

Brum, G., Ríos, E. & Stefani, E. (1988). Effects of extracellular calcium on calcium movements of excitation–contraction coupling in frog skeletal muscle fibres. *Journal of Physiology* **398**, 441–473.

Cannell, M. B., Berlin, J. R. & Lederer, W. J. (1987). Effect of membrane potential changes on the calcium transient in single rat cardiac muscle cells. *Science* **238**, 1419–1423.

Cannell, M. B., Cheng, H. & Lederer, W. J. (1994). Spatial non-uniformities in $[Ca^{2+}]_\mathrm{i}$ during excitation-contraction coupling in cardiac myocytes. *Biophysical Journal* **67**, 1942–1956.

Cannell, M. B., Cheng, H. & Lederer, W. J. (1995). The control of calcium release in heart muscle. *Science* **268**, 1045–1049.

Cheng, H., Cannell, M. B. & Lederer, W. J. (1994). Propagation of excitation-contraction coupling into ventricular myocytes. *Pflügers Archiv* **428**, 415–417.

Cheng, H., Cannell, M. B. & Lederer, W. J. (1995). Partial inhibition of Ca^{2+} current by methoxyverapamil (D600) reveals spatial nonuniformities in $[Ca^{2+}]_\mathrm{i}$ during excitation-contraction coupling in cardiac myocytes. *Circulation Research* **76**, 236–241.

Cheng, H., Lederer, W. J. & Cannell, M. B. (1993). Calcium sparks: elementary events underlying excitation-contraction coupling in heart muscle. *Science* **262**, 740–744.

Cheng, H., Lederer, M. R., Lederer, W. J. & Cannell, M. B. (1996). Calcium sparks and $[Ca^{2+}]_\mathrm{i}$ waves in cardiac myocytes. *American Journal of Physiology* **270**, C148–159.

Cleemann, L. & Morad, M. (1991). Role of Ca^{2+} channel in cardiac excitation–contraction coupling in the rat: evidence from Ca^{2+} transients and contraction. *Journal of Physiology* **432**, 283–312.

Crespo, L. M., Grantham, C. J. & Cannell, M. B. (1990). Kinetics, stoichiometry and role of the Na-Ca exchange mechanism in isolated cardiac myocytes. *Nature* **345**, 618–621.

Ehrhardt, D. W., Wais, R. & Long, S. R. (1996). Calcium spiking in plant root hairs responding to *Rhizobium* nodulation signals. *Cell* **85**, 673–681.

Escobar, A. L., Cifuentes, F. & Vergara, J. L. (1995). Detection of Ca^{2+}-transients elicited by flash photolysis of DM-nitrophen with a fast calcium indicator. *FEBS Letters* **364**, 335–338.

Escobar, A. L., Monck, J. R., Fernandez, J. M. & Vergara, J. L. (1994). Localization of the site of Ca^{2+} release at the level of a single sarcomere in skeletal muscle fibres. *Nature* **367**, 739–741.

Fabiato, A. (1985). Time and calcium dependence of activation and inactivation of calcium-induced release of calcium from the sarcoplasmic reticulum of a skinned canine cardiac Purkinje cell. *Journal of General Physiology* **85**, 247–289.

Györke, S. & Fill, M. (1993). Ryanodine receptor adaptation: control mechanism of Ca^{2+}-induced Ca^{2+} release in heart. *Science* **260**, 807–809.

Isenberg, G., Etter, E. F., Wendt-Gallitelli, M. F., Schiefer, A., Carrington, W. A., Tuft, R. A. & Fay, F. S. (1996). Intrasarcomere $[Ca^{2+}]$ gradients in ventricular myocytes revealed by high speed digital imaging microscopy. *Proceedings of the National Academy of Sciences of the USA* **93**, 5413–5418.

Klein, M. G., Cheng, H., Santana, L. F., Jiang, Y. H., Lederer, W. J. & Schneider, M. F. (1996). Two mechanisms of quantized calcium release in skeletal muscle. *Nature* **379**, 455–458.

Langer, G. A. & Peskoff, A. (1996). Calcium concentration and movement in the diadic cleft space of the cardiac ventricular cell. *Biophysical Journal* **70**, 1169–1182.

Lechleiter, J. D. & Clapham, D. E. (1992). Molecular mechanisms of intracellular calcium excitability in *X. laevis* oocytes. *Cell* **69**, 283–294.

López-López, J. R., Shacklock, P. S., Balke, C. W. & Wier, W. G. (1994). Local, stochastic release of Ca^{2+} in voltage-clamped rat heart cells: visualization with confocal microscopy. *Journal of Physiology* **480**, 21–29.

López-López, J. R., Shacklock, P. S., Balke, C. W. & Wier, W. G. (1995). Local calcium transients triggered by single L-type calcium channel currents in cardiac cells. *Science* **268**, 1042–1045.

Melzer, W., Ríos, E. & Schneider, M. F. (1986). The removal of myoplasmic free calcium following calcium release in frog skeletal muscle. *Journal of Physiology* **372**, 261–292.

Niggli, E. & Lederer, W. J. (1990). Voltage-independent calcium release in heart muscle. *Science* **250**, 565–568.

Ríos, E. & Pizarro, G. (1991). Voltage sensor of excitation-contraction coupling in skeletal muscle. *Physiological Reviews* **71**, 849–908.

Santana, L. F., Cheng, H., Gomez, A. M., Cannell, M. B. & Lederer, W. J. (1996). Relation between the sarcolemmal Ca^{2+} current and Ca^{2+} sparks and local control theories for cardiac excitation-contraction coupling. *Circulation Research* **78**, 166–171.

Shacklock, P. S., Wier, W. G. & Balke, C. W. (1995). Local Ca^{2+} transients (Ca^{2+} sparks) originate at transverse tubules in rat heart cells. *Journal of Physiology* **487**, 601–608.

Sham, J. S. (1997). Ca^{2+} release-induced inactivation of Ca^{2+} current in rat ventricular myocytes: evidence for local Ca^{2+} signalling. *Journal of Physiology* **500**, 285–295.

Sham, J. S., Cleemann, L. & Morad, M. (1995). Functional coupling of Ca^{2+} channels and ryanodine receptors in cardiac myocytes. *Proceedings of the National Academy of Sciences of the USA* **92**, 121–125.

Sham, J. S., Song, L. S., Chen, Y., Deng, L. H., Stern, M. D., Lakatta, E. G. & Cheng, H. (1998). Termination of Ca^{2+} release by local inactivation of ryanodine receptors in cardiac myocytes. *Proceedings of the National Academy of Sciences of the USA* (in the Press).

Shmigol, A., Verkhratsky, A. & Isenberg, G. (1995). Calcium-induced calcium release in rat sensory neurons. *Journal of Physiology* **489**, 627–636.

Sipido, K. R. & Wier, W. G. (1991). Flux of Ca^{2+} across the sarcoplasmic reticulum of guinea-pig cardiac cells during excitation–contraction coupling. *Journal of Physiology* **435**, 605–630.

Smith, G. D., Keizer, J. E., Stern, M. D., Lederer, W. J. & Cheng, H. (1998). A simple numerical model of calcium spark formation and detection in cardiac myocytes. *Biophysical Journal* **75**, 15–32.

Soeller, C. & Cannell, M. B. (1997). Numerical simulation of local calcium movements during L-type calcium channel gating in the cardiac diad. *Biophysical Journal* **73**, 97–111.

Song, L. S., Stern, M. D., Lakatta, E. G. & Cheng, H. (1997). Partial depletion of sarcoplasmic reticulum calcium does not prevent calcium sparks in rat ventricular myocytes. *Journal of Physiology* **505**, 665–675.

Spurgeon, H. A., Stern, M. D., Baartz, G., Raffaeli, S., Hansford, R. G., Talo, A., Lakatta, E. G. & Capogrossi, M. C. (1990). Simultaneous measurement of Ca^{2+}, contraction, and potential in cardiac myocytes. *American Journal of Physiology* **258**, H574–586.

Stern, M. D. (1992*a*). Theory of excitation-contraction coupling in cardiac muscle. *Biophysical Journal* **63**, 497–517.

Stern, M. D. (1992*b*). Buffering of calcium in the vicinity of a channel pore. *Cell Calcium* **13**, 183–192.

Wier, W. G. (1990). Cytoplasmic [Ca^{2+}] in mammalian ventricle: dynamic control by cellular processes. *Annual Review of Physiology* **52**, 467–485.

Wier, W. G., Cannell, M. B., Berlin, J. R., Marban, E. & Lederer, W. J. (1987). Cellular and subcellular heterogeneity of $[Ca^{2+}]_i$ in single heart cells revealed by fura-2. *Science* **235**, 325–328.

Wier, W. G., Egan, T. M., López-López, J. R. & Balke, C. W. (1994). Local control of excitation–contraction coupling in rat heart cells. *Journal of Physiology* **474**, 463–471.

Xiao, R. P., Valdivia, H. H., Bogdanov, K., Valdivia, C., Lakatta, E. G. & Cheng, H. (1997). The immunophilin FK506-binding protein modulates Ca^{2+} release channel closure in rat heart. *Journal of Physiology* **500**, 343–354.

Yue, D. T. & Wier, W. G. (1985). Estimation of intracellular [Ca^{2+}] by nonlinear indicators. A quantitative analysis. *Biophysical Journal* **48**, 533–537.

Ziegelstein, R. C., Spurgeon, H. A., Pili, R., Passaniti, A., Cheng, L., Corda, S., Lakatta, E. G. & Capogrossi, M. C. (1994). A functional ryanodine-sensitive intracellular Ca^{2+} store is present in vascular endothelial cells. *Circulation Research* **74**, 151–156.

Acknowledgements

The authors acknowledge the expert technical support from Dr Harold Spurgeon and Bruce Ziman. H.C. would like to thank Dr J. L. Vergara for discussion on the use of low-affinity dye. This work was supported by NIH Intramural Research Program (H.C., M.D.S. and E.G.L.) and extramural grants (HL-52652, J.S.K.S.) and AHA Established Investigator Award (J.S.K.S.).

Corresponding authors

H. Cheng: Laboratory of Cardiovascular Science, Gerontology Reasearch Center, National Institute on Aging, National Institutes of Health, 5600 Nathan Shock Drive, Baltimore, MD 21224, USA.

Email: chengp@grc.nia.nih.gov

J. S. K. Sham: Division of Pulmonary and Critical Care Medicine, Johns Hopkins Medical Institutions, 5501 Hopkins Bayview Circle, Baltimore, MD21224, USA.

Email: jsks@welchlink.welch.jhu.edu